Supplementary Information

Proximity Matters: Interfacial Solvation Dictates Solid Electrolyte Interphase Composition

Solomon T. Oyakhire[1], Sheng-Lun Liao[1], Sanzeeda Baig Shuchi[1], Mun Sek Kim[1,2], Sang Cheol Kim[2], Zhiao Yu[3], Rafael A. Vilá[2], Paul E. Rudnicki[1], Yi Cui[*2,4,5], Stacey F. Bent[*1,4]

1 Department of Chemical Engineering, Stanford University, Stanford, CA 94305, USA.

2 Department of Materials Science and Engineering, Stanford University, Stanford, CA 94305, USA.

3 Department of Chemistry, Stanford University, Stanford, CA 94305, USA.

4 Department of Energy Science and Engineering, Stanford University, Stanford, CA 94305, USA.

5 Stanford Institute for Materials and Energy Sciences, SLAC National Accelerator Laboratory, 2575 Sand Hill Road, Menlo Park, CA 94025, USA.

* Email: yicui@stanford.edu

* Email: sbent@stanford.edu

Methods

Film deposition

The Al_2O_3 film was deposited using trimethylaluminum (TMA) as the metal-organic precursor and water (H_2O) as the counter reactant. An ALD scheme of 1/30/1/30 s TMA pulse/purge/H_2O pulse/purge sequence at 120 °C was used, resulting in a growth of 1.1 Å per cycle. The deposition was conducted directly on a Cu foil in a Gemstar 6 ALD reactor (Arradiance). The thickness of the film was determined by growth on a reference Si wafer, using a J.A. Woollam M2000 Variable Angle Spectroscopic Ellipsometer at 65° and 70° angles of incidence and wavelengths ranging from 210 to 1688nm.

Materials

All electrolytes used in this study were prepared and handled in an Ar-filled glove box in which O_2 concentration was below 0.2 ppm, and H_2O concentration was below 0.01 ppm. The 1 M lithium hexafluorophosphate ($LiPF_6$) in 1:1 volume ratio of ethylene carbonate (EC) and diethyl carbonate (DEC) (LP40) electrolyte was purchased and used as received from Gotion. The 1 M lithium bisfluorosulfonyl imide (LiFSI) in dimethoxyethane (DME) electrolyte was prepared using LiFSI purchased from Oakwood and DME purchased from Aldrich. The F5DEE solvent was synthesized as reported in a previous publication.[1] The 1.2 M LiFSI F5DEE electrolyte was prepared by dissolving LiFSI salt (Oakwood) in F5DEE solvent. High-purity Li foil (0.75 mm, 99.9% Alfa Aesar), Cu foil (Pred Materials), and polymer separator (Celgard 2325) were used to make cells in Li||Cu configurations for electrochemical tests, microscopy, and spectroscopy measurements.

Electrochemistry

Type 2032 coin cells were assembled in an argon glovebox with a polymer separator (Celgard 2325). Li metal foil (0.75 mm thick, 99.9% Alfa Aesar) was used as the counter/reference electrode and a Cu foil was used as the working electrode. Li was mechanically sheared to remove surface oxides while Cu foil was rinsed with acetone, isopropyl alcohol, and deionized water to remove surface contaminants prior to cell assembly. The Li||Cu configuration was used for cyclability and XPS characterizations. All Li||Cu cells were cycled at 25 ˚C on an Arbin battery cycler using the corresponding Li deposition current densities stated in the main text and Li stripping was performed with a cutoff voltage of 1 V vs Li^+/Li. 60 µL of

electrolyte was used for standard Li||Cu CE measurements which involve Li deposition at a fixed current density and total capacity and Li stripping at a fixed current density and cutoff voltage. The Aurbach CE measurements were carried out at 0.5 mA/cm^2 using a standard protocol developed in a previous report[2]: 5 mAh of Li was first deposited and stripped, then 5 mAh of Li was redeposited and 1 mAh of this redeposited Li was cycled 10 times before a final stripping cycle to 1 V vs Li^+/Li. 40 µL of electrolyte was used for Aurbach CE measurements. Li||Cu cells were used for EIS measurements after Li deposition on Cu under the current density conditions listed in the main text; 60 µL of electrolyte was used for aging and impedance experiments. The initial impedance measurements were carried out 5 minutes after lithium deposition, and impedance was continuously measured for 12 hours after the initial measurements. Impedance measurements were carried out under open-circuit conditions within a frequency range of 1 MHz to 100 mHz, with a perturbation amplitude of 5 mV, using a Biologic VMP3 potentiostat.

XPS characterization

After fresh lithium deposition or SEI formation on Cu foil working electrodes, the electrodes were prepared in an Ar glove box and rinsed with 90 µL of pure solvents (diethyl carbonate for LP40, and 1,2 dimethoxy ethane for the DME and FDMB electrolytes) to remove residual Li salts, then transferred to an XPS chamber using a vacuum transfer vessel. XPS signals were collected on a PHI VersaProbe 1 scanning XPS microprobe with an Al Kα source and elemental spectra were shifted with reference to a C 1s binding energy of 284.6 eV.

MD simulations

MD simulations were carried out using Gromacs 2021.3[3] with the optimized potentials for liquid simulations all-atom force field[4] for the LP40 electrolyte and the interface force field for Cu and Al_2O_3 slabs[5]. Topology files and Lennard-Jones parameters for carbonates were generated using the LigParGen server,[6] while parameters for $PF6^-$ were extracted from literature.[7]

The dimensions of the simulation boxes are 5.13 x 4.76 x 11.90 and 5.12 x 5.32 x 11.21 (nm^3) for Al_2O_3 and Cu systems, and the thicknesses of the Al_2O_3 and Cu slabs are approximately 1.20 and 1.47 nm, respectively. Both systems contain the same number of EC, DEC, and $PF6^-$ molecules. To mimic the amorphous/heterogenous experimental structures of the slabs, we designed non-perfect simulation slab crystals by heating the system of slab and electrolyte up to 1000 K within 2 ns, then annealed the system at 300 K for 10 ns. Subsequently, a 40 ns equilibration step was applied, followed by a 40 ns production run using the Parrinello–Rahman barostat with the Nosé-Hoover thermostat. Semi-isotropic pressure coupling was specified for barostat such that the systems were only allowed to compress in the direction perpendicular to the slabs with a reference pressure of 1 bar. A Nosé-Hoover thermostat was used throughout with a reference temperature of 300 K. All the results presented were generated from the final 40 ns of the production run. The particle mesh Ewald method was used to calculate electrostatic interactions, with a real-space cut-off of 1 nm and a Fourier spacing of 0.16 nm. The Verlet cut-off scheme was used to generate pair lists. A cut-off of 1 nm was used for non-bonded Lennard-Jones interactions. Periodic boundary conditions were applied in all directions and bonds with hydrogen atoms were constrained.

The visualizations were generated with VMD.[8] Solvation statistics were calculated using the MDAnalysis Python package[9,10] and a histogram was used to analyze probability density in the distance between molecules and slab.

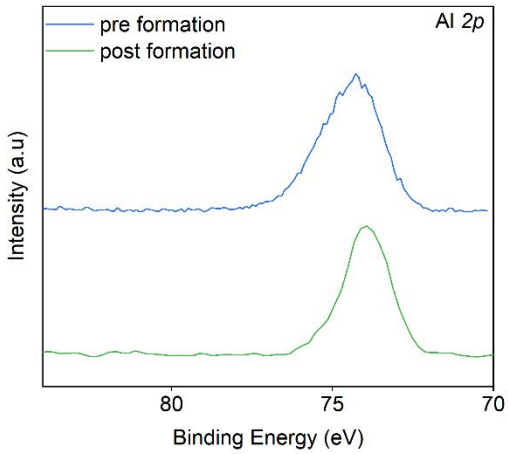

Supplementary Figure 1. Representative XPS spectra of Al_2O_3 collected before and after 24-hour SEI formation.

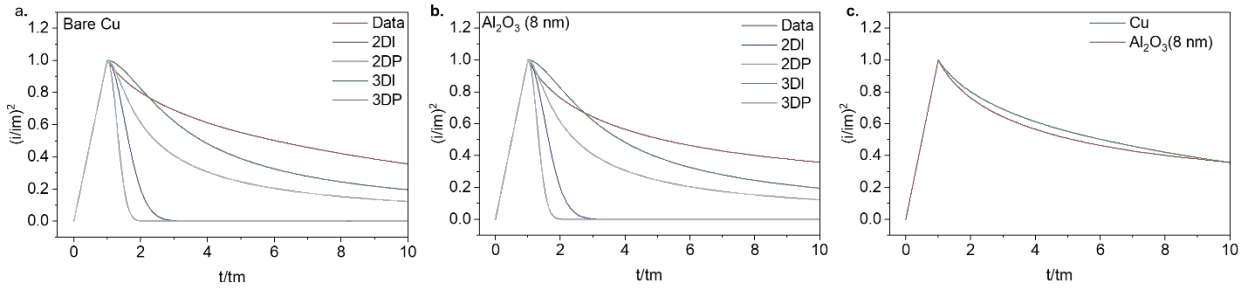

Supplementary Figure 2. SEI nucleation and growth mechanisms. a,b Dimensionless trends of current versus time for SEIs formed on Cu and Al_2O_3 in LP40 electrolyte, respectively. Trends are compared with two-dimensional (2D) and three-dimensional (3D) (I= instantaneous and P = progressive) models of nucleation and growth[11,12] c. Dimensionless trends of current versus time for SEI formation on Cu and 8 nm Al_2O_3 in LP40 electrolyte.

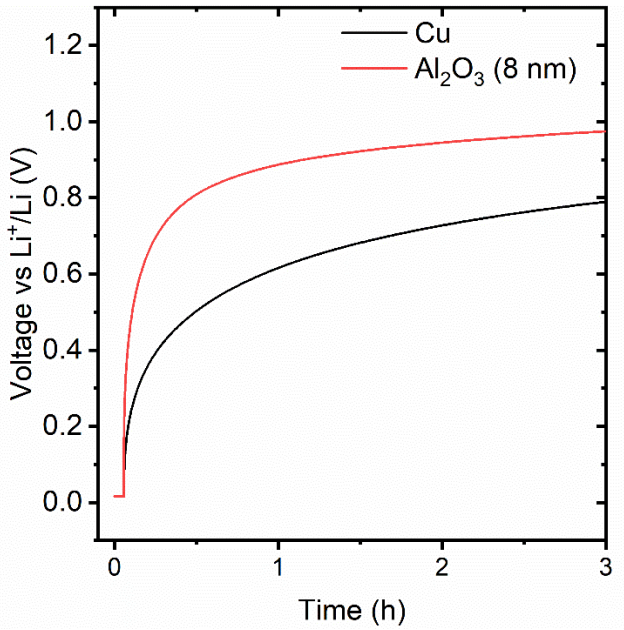

Supplementary Figure 3. Voltage relaxation tests showing substrate voltage vs Li^+/Li after 1 hour of SEI formation in LP40 on different substrates.

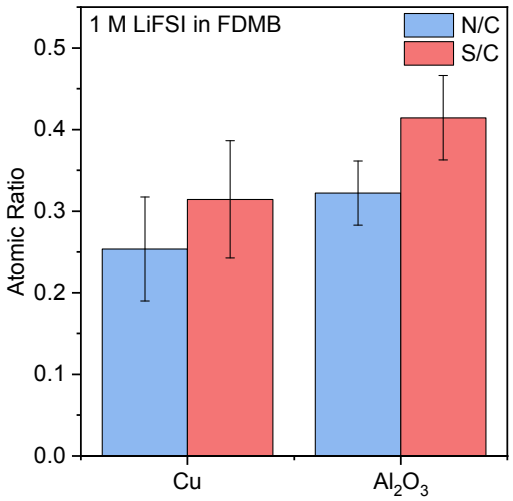

Supplementary Figure 4. Atomic ratio of SEIs formed after 24 hours on Cu and 8 nm Al_2O_3 substrates in 1 M LiFSI FDMB[13] electrolyte.

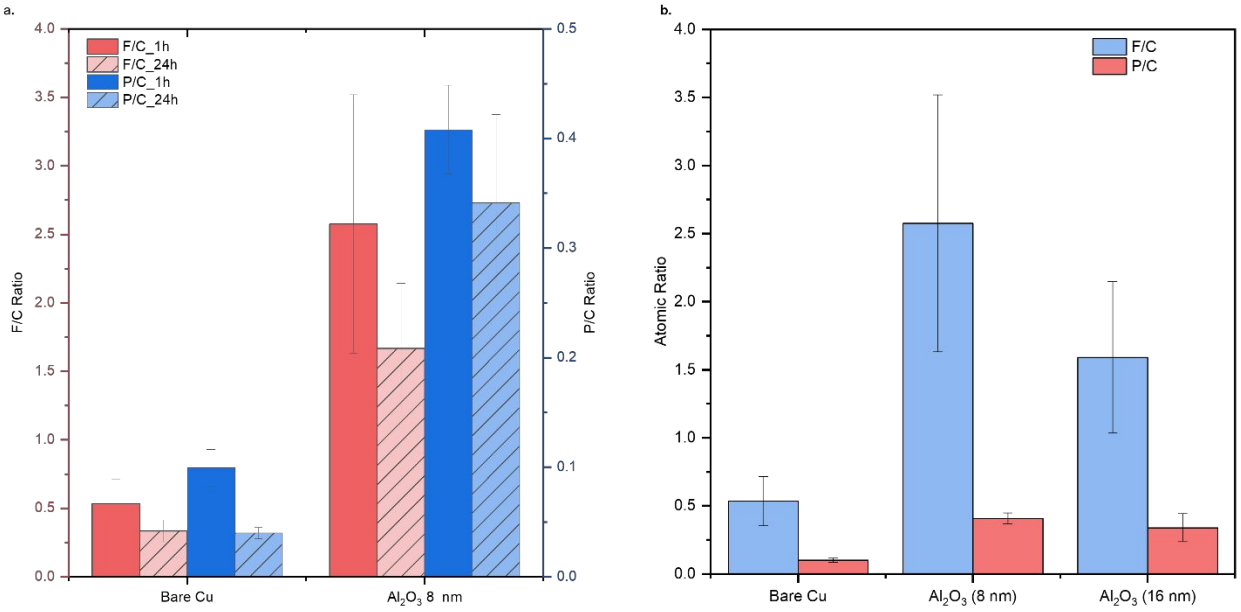

Supplementary Figure 5. a. Atomic ratio of SEIs formed after 1 hour and 24 hours on Cu and 8 nm Al_2O_3 substrates in LP40. b. Atomic ratio of SEIs formed after 1 hour on Cu and Al_2O_3 substrates of different thicknesses in LP40.

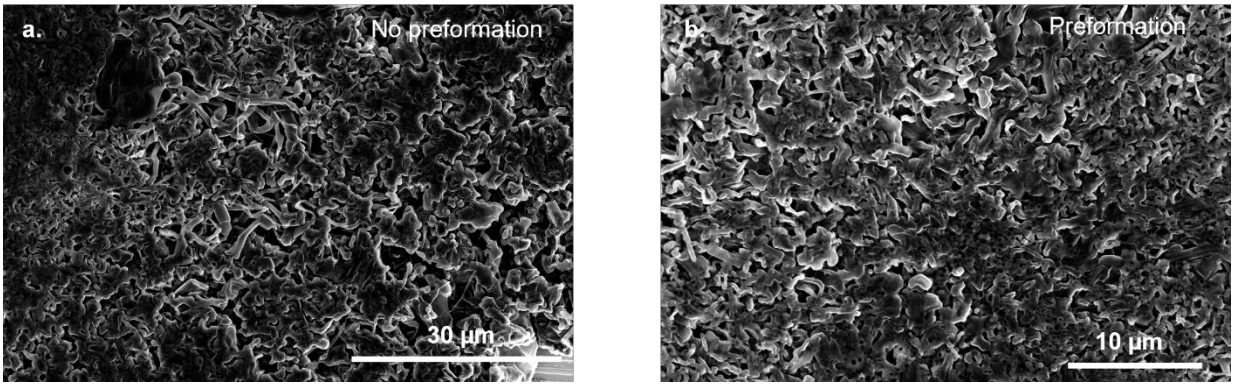

Supplementary Figure 6. a,b Morphology of 0.5 mAh/cm^2 of Li deposited using LP40 on 8 nm Al_2O_3 substrates without and with SEI preformation, respectively.

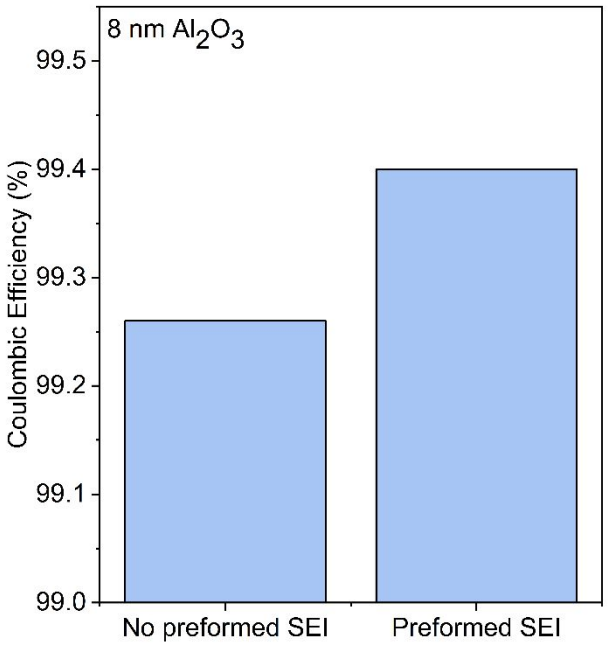

Supplementary Figure 7. Aurbach CE measurements for 8 nm Al_2O_3 substrates with and without preformed SEIs tested in 1.2 M LiFSI F5DEE at 0.5 mA/cm^2. Reported CEs were obtained by taking averages over at least two cells.

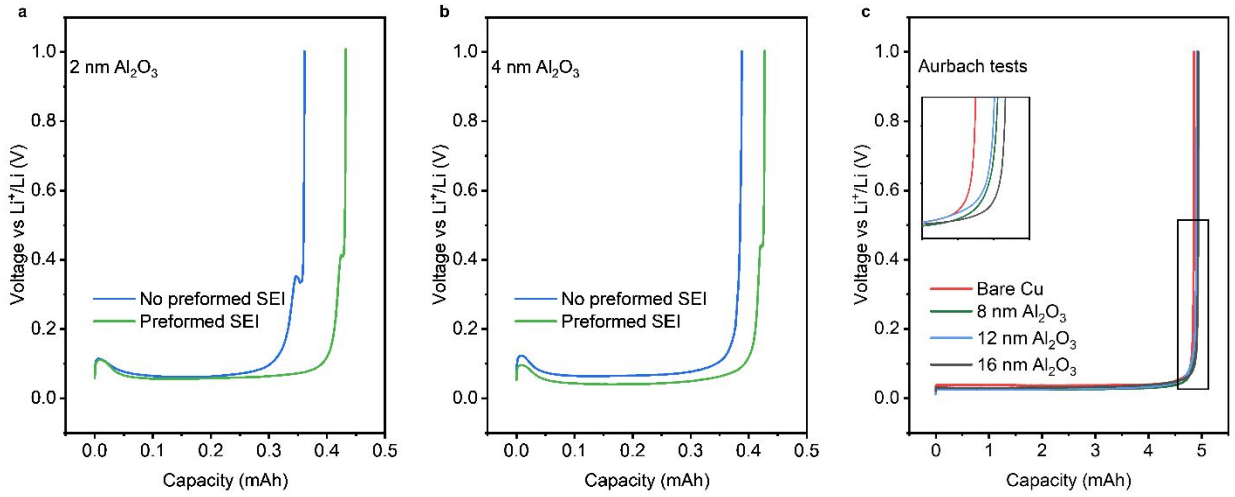

Supplementary Figure 8. Representative voltage profiles showing the performance benefits of SEI preformation a,b Lithium stripping profile after one cycle of deposition on 2 nm and 4 nm Al_2O_3 films in LP40 electrolyte. c. Lithium stripping profile after Aurbach tests on different thicknesses of Al_2O_3 carried out using F5DEE electrolyte.

Supplementary Note 1

SEI formation usually follows 2D, 3D, or hybrid 2D-3D mechanistic paths. Theoretical models for 2D and 3D nucleation and growth have been developed in studies by Bewick et al.[12] and Scharifker et al.[11], respectively. In 2D formation, nucleation occurs across the x-y plane of the substrate, then growth progresses in the z direction only after one monolayer of the x-y plane is covered. As such, 2D growth typically results in uniform layers of films that grow stepwise, in the z direction. In 3D formation, nucleation also occurs across the x-y plane, however, growth progresses in the z-direction before the x-y plane is fully covered. As a result, 3D growth typically results in islands and partially covered substrates. In addition, 2D and 3D mechanisms can also follow either instantaneous or progressive paths. Instantaneous paths are indicative of fast nucleation kinetics, while progressive paths reflect slow nucleation kinetics. The dimensionless forms of the models for SEI formation are expressed as follows:

$$\frac{i}{i_m} = \left(\frac{t}{t_m}\right)\exp\left(0.5\left(1-\left(\left(\frac{t}{t_m}\right)^2\right)\right)\right) \quad \text{2D-instantaneous model}$$

$$\frac{i}{i_m} = \frac{t}{t_m}^2 \exp\left(\frac{2}{3}\left(1-\left(\left(\frac{t}{t_m}\right)^2\right)\right)\right) \quad \text{2D-progressive model}$$

$$\frac{i}{i_m} = \left(1.9542\frac{t_m}{t}\right)^{0.5}\left(1-\exp\left(-1.2564\frac{t}{t_m}\right)\right) \quad \text{3D-instantaneous model}$$

$$\frac{i}{i_m} = \left(1.2254\frac{t_m}{t}\right)^{0.5}\left(1-\exp\left(2.3367\frac{t}{t_m}\right)\right)^2 \quad \text{3D-progressive model}$$

Where i represents current, i_m represents maximum current during SEI formation, t represents time, and t_m represents time at which current is maximum.

Based on the data presented in **Supplementary Figures 2a and 2b**, the SEI formation mechanism on both Cu and Al_2O_3 substrates does not perfectly match any of the established formation models, but it appears most similar to the 3D-instantaneous model, suggesting that SEI islands form atop both

substrates. Deriving new models to account for the exact SEI formation mechanism atop both substrates is beyond the scope of this work, but it is important to note that both substrates exhibit similar mechanisms as shown in **Supplementary Figure 2c**.

References

(1) Yu, Z.; Rudnicki, P. E.; Zhang, Z.; Huang, Z.; Celik, H.; Oyakhire, S. T.; Chen, Y.; Kong, X.; Kim, S. C.; Xiao, X.; Wang, H.; Zheng, Y.; Kamat, G. A.; Kim, M. S.; Bent, S. F.; Qin, J.; Cui, Y.; Bao, Z. Rational Solvent Molecule Tuning for High-Performance Lithium Metal Battery Electrolytes. *Nat. Energy* **2022**, *7* (1), 94–106. https://doi.org/10.1038/s41560-021-00962-y.

(2) Adams, B. D.; Zheng, J.; Ren, X.; Xu, W.; Zhang, J.-G. G. Accurate Determination of Coulombic Efficiency for Lithium Metal Anodes and Lithium Metal Batteries. *Adv. Energy Mater.* **2018**, *8* (7), 1702097. https://doi.org/10.1002/aenm.201702097.

(3) Abraham, M. J.; Murtola, T.; Schulz, R.; Páll, S.; Smith, J. C.; Hess, B.; Lindah, E. Gromacs: High Performance Molecular Simulations through Multi-Level Parallelism from Laptops to Supercomputers. *SoftwareX* **2015**, *1–2*, 19–25. https://doi.org/10.1016/j.softx.2015.06.001.

(4) Jorgensen, W. L.; Maxwell, D. S.; Tirado-Rives, J. Development and Testing of the OPLS All-Atom Force Field on Conformational Energetics and Properties of Organic Liquids. *J. Am. Chem. Soc.* **1996**, *118* (45), 11225–11236. https://doi.org/10.1021/ja9621760.

(5) Heinz, H.; Lin, T. J.; Kishore Mishra, R.; Emami, F. S. Thermodynamically Consistent Force Fields for the Assembly of Inorganic, Organic, and Biological Nanostructures: The INTERFACE Force Field. *Langmuir* **2013**, *29* (6), 1754–1765. https://doi.org/10.1021/la3038846.

(6) Dodda, L. S.; De Vaca, I. C.; Tirado-Rives, J.; Jorgensen, W. L. LigParGen Web Server: An Automatic OPLS-AA Parameter Generator for Organic Ligands. *Nucleic Acids Res.* **2017**, *45* (W1), W331–W336. https://doi.org/10.1093/nar/gkx312.

(7) Doherty, B.; Zhong, X.; Gathiaka, S.; Li, B.; Acevedo, O. Revisiting OPLS Force Field Parameters for Ionic Liquid Simulations. *J. Chem. Theory Comput.* **2017**, *13* (12), 6131–6135. https://doi.org/10.1021/acs.jctc.7b00520.

(8) Humphrey, W.; Dalke, A.; Schulten, K. VMD: Visual Molecular Dynamics. *J. Mol. Graph.* **1996**, *14* (1), 33–38. https://doi.org/10.1016/0263-7855(96)00018-5.

(9) Gowers, R.; Linke, M.; Barnoud, J.; Reddy, T.; Melo, M.; Seyler, S.; Domański, J.; Dotson, D.; Buchoux, S.; Kenney, I.; Beckstein, O. MDAnalysis: A Python Package for the Rapid Analysis of Molecular Dynamics Simulations. In *Proceedings of the 15th Python in Science Conference*; 2016; pp 98–105. https://doi.org/10.25080/majora-629e541a-00e.

(10) Michaud-Agrawal, N.; Denning, E. J.; Woolf, T. B.; Beckstein, O. MDAnalysis: A Toolkit for the Analysis of Molecular Dynamics Simulations. *J. Comput. Chem.* **2011**, *32* (10), 2319–2327. https://doi.org/10.1002/jcc.21787.

(11) Scharifker, B.; Hills, G. Theoretical and Experimental Studies of Multiple Nucleation. *Electrochim. Acta* **1983**, *28* (7), 879–889. https://doi.org/10.1016/0013-4686(83)85163-9.

(12) Bewick, A.; Fleischmann, M.; Thirsk, H. R. Kinetics of the Electrocrystallization of Thin Films of Calomel. *Trans. Faraday Soc.* **1962**, *58* (0), 2200–2216. https://doi.org/10.1039/tf9625802200.

(13) Yu, Z.; Wang, H.; Kong, X.; Huang, W. W.; Tsao, Y.; Mackanic, D. G.; Wang, K.; Wang, X.;

Huang, W. W.; Choudhury, S.; Zheng, Y.; Amanchukwu, C. V.; Hung, S. T.; Ma, Y.; Lomeli, E. G.; Qin, J.; Cui, Y.; Bao, Z. Molecular Design for Electrolyte Solvents Enabling Energy-Dense and Long-Cycling Lithium Metal Batteries. *Nat. Energy* **2020**, *5* (7), 526–533. https://doi.org/10.1038/s41560-020-0634-5.